JGP Journal of General Physiology

ARTICLE

Myosin expression and contractile function are altered by replating stem cell–derived cardiomyocytes

Felix Osten[1*], Natalie Weber[1,2*], Meike Wendland[1], Tim Holler[1], Birgit Piep[1], Simon Kröhn[1], Jana Teske[3], Alea K. Bodenschatz[1], Santoshi Biswanath Devadas[3], Kaja S. Menge[2], Shambhabi Chatterjee[2], Kristin Schwanke[3], Maike Kosanke[4], Judith Montag[1], Thomas Thum[2,5,6], Robert Zweigerdt[3], Theresia Kraft[1], Bogdan Iorga[1,7**], and Joachim D. Meissner[1**]

Myosin heavy chain (MyHC) is the main determinant of contractile function. Human ventricular cardiomyocytes (CMs) predominantly express the β-isoform. We previously demonstrated that ∼80% of human embryonic stem cell–derived cardiomyocytes (hESC-CMs) express exclusively β-MyHC after long-term culture on laminin-coated glass coverslips. Here, we investigated the impact of enzymatically detaching hESC-CMs after long-term culture and subsequently replating them for characterization of cellular function. We observed that force-related kinetic parameters, as measured in a micromechanical setup, resembled α- rather than β-MyHC-expressing myofibrils, as well as changes in calcium transients. Single-cell immunofluorescence analysis revealed that replating hESC-CMs led to rapid upregulation of α-MyHC, as indicated by increases in exclusively α-MyHC- and in mixed α/β-MyHC-expressing hESC-CMs. A comparable increase in heterogeneity of MyHC isoform expression was also found among individual human induced pluripotent stem cell (hiPSC)–derived CMs after replating. Changes in MyHC isoform expression and cardiomyocyte function induced by replating were reversible in the course of the second week after replating. Gene enrichment analysis based on RNA-sequencing data revealed changes in the expression profile of mechanosensation/-transduction-related genes and pathways, especially integrin-associated signaling. Accordingly, the integrin downstream mediator focal adhesion kinase (FAK) promoted β-MyHC expression on a stiff matrix, further validating gene enrichment analysis. To conclude, detachment and replating induced substantial changes in gene expression, MyHC isoform composition, and function of long-term cultivated human stem cell–derived CMs, thus inducing alterations in mechanosensation/-transduction, that need to be considered, particularly for downstream in vitro assays.

Introduction

Human adult ventricular CMs predominantly express β-MyHC, encoded by *MYH7*, whereas atrial CMs express predominantly α-MyHC, encoded by *MYH6* (Reiser et al., 2001). Myosin heavy chain (MyHC) isoform expression is the main determinant of contractility and power output of the heart (Herron and McDonald, 2002; Palmiter et al., 1999; Schwartz et al., 1981). Related to a higher ATPase activity of α-MyHC, the speed of myocardial contraction (Schwartz et al., 1981) and peak normalized power output (Herron and McDonald, 2002) are higher in CMs containing a higher amount of α-MyHC and crossbridge kinetics are faster with a higher amount of α-MyHC (Rundell et al., 2005).

Human pluripotent stem cell-derived cardiomyocytes (hPSC-CMs) have great potential for therapeutic applications in regenerative medicine, pharmacological studies, and as models for cardiac disease or cardiomyocyte development (Yang et al., 2014). It has been shown that the phenotype of hPSC-CMs differs substantially from adult human CMs in gene expression, morphology, and function, despite considerable progress in differentiation protocols (Denning et al., 2016). One of several

[1]Institute of Molecular and Cell Physiology, Hannover Medical School, Hannover, Germany; [2]Institute of Molecular and Translational Therapeutic Strategies (IMTTS), Hannover Medical School, Hannover, Germany; [3]Department of Cardiothoracic, Transplantation and Vascular Surgery, Leibniz Research Laboratories for Biotechnology and Artificial Organs (LEBAO), Hannover Medical School, Hannover, Germany; [4]Research Core Unit Genomics, Hannover Medical School, Hannover, Germany; [5]REBIRTH Center for Translational Regenerative Therapies, Hannover Medical School, Hannover, Germany; [6]Fraunhofer Institute for Toxicology and Experimental Medicine, Hannover, Germany; [7]Department of Analytical Chemistry and Physical Chemistry, Faculty of Chemistry, University of Bucharest, Bucharest, Romania.

*F. Osten and N. Weber contributed equally to this paper; **B. Iorga and J.D. Meissner contributed equally to this paper.
Correspondence to Felix Osten: osten.felix@mh-hannover.de

S. Kröhn's current address is Clinic for Nuclear Medicine, Hannover Medical School, Hannover, Germany.

distinct strategies to improve in vitro maturation of hPSC-CMs is long-term culture on a stiff matrix (Yang et al., 2014). We have previously shown that the number of exclusively the β-isoform of MyHC expressing human embryonic stem cell–derived cardiomyocytes (hESC-CMs) increases to over 80% after long-term culture on laminin-coated glass coverslips, i.e., a stiff matrix, while no exclusively α-MyHC expressing CMs were found (Weber et al., 2016). Cultivation in a soft environment as cardiac bodies (CB) in suspension culture for the same time yields only ∼10% of exclusively β-MyHC expressing CMs, while the rest express mainly α-MyHC (Weber et al., 2016). Therefore, long-term culture of hESC-CMs on a stiff matrix promotes the maturation of hESC-CMs to a fairly homogenous culture with ventricular phenotype with respect to the level of MyHC isoform expression. Nevertheless, the maturation state of hPSC-CMs is also determined by the expression of other genes as well as morphological and functional characteristics (Jiang et al., 2018).

Yet, in models for cardiac disease or cardiomyocyte development (Yang et al., 2014), CMs are often detached from their substrate after short-, middle-, or long-term culture and shortly replated for further analyses. We aimed to investigate whether enzymatically detaching and replating hESC-CMs has an impact on hESC-CM function. Detachment of cells from the substrate can have profound effects on gene expression and cell function. For example, detachment has been shown to influence signaling pathways that are involved in the regulation of contractile activity during cell migration (Ren et al., 2004). In addition, it has been demonstrated that different combinations of detachment reagents and the replating matrix had differential effects on hiPSC-CMs in terms of recovery and viability (Koc et al., 2021).

Detachment and replating of CMs are considered to be associated with a change in the stiffness of the matrix. In vivo, adaptations to an altered mechanical environment, mediated by cellular mechanosensation/-transduction and its downstream effects, are well known to lead to cardiomyocyte remodeling under physiological and pathophysiological conditions (Saucerman et al., 2019). In CMs, integrins have been shown to play a crucial role in mechanotransduction by linking the extracellular matrix (ECM) to intracellular signaling (Israeli-Rosenberg et al., 2014; Pentassuglia and Sawyer, 2013). In the regulation of myocardial cell–cell and cell–matrix interactions, focal adhesion kinase (FAK) is a crucial downstream mediator of integrins. Among a variety of factors, the extracellular signal-regulated kinase (ERK) 1/2, a member of the mitogen-activated protein kinases (MAPKs), is involved in further downstream integrin/FAK signaling. Integrins and FAK play important roles in cardiac development and disease and have further been shown to be involved in the differentiation of induced pluripotent stem cells into CMs (Castillo et al., 2020; Santoro et al., 2019).

In this study, evaluation of the MyHC isoform expression profile of replated hESC-CMs, as well as replated human induced pluripotent stem cell-derived (hiPSC) CMs, demonstrated a rather rapid shift from β- to α-MyHC expression. This shift was associated with functional changes. Alterations in MyHC isoform expression and contractile function were shown to be reversible in the second week after replating. Furthermore, expression of genes related to mechanosensation/-transduction, especially integrin-associated signaling, was also altered in replated hESC-CMs. In line, inhibition of the integrin downstream mediator FAK decreased β-MyHC expression. Changes in gene expression, especially of integrin-associated signaling pathways, suggest that alterations in mechanosensation/-transduction induce changes in MyHC isoform expression and CM function upon detaching and replating of hPSC-CMs.

Materials and methods

Differentiation, genetic cardiomyocyte enrichment, and cultivation of hESC-CMs

Differentiation, genetic CM-enrichment, and cultivation of hESC-CMs were performed as described previously (Fig. 1; Schwanke et al., 2014; Weber et al., 2016; Xu et al., 2008). Briefly, suspension-derived CBs were dissociated at day 12–20 using Collagenase B (Roche). CBs were washed with phosphate-buffered saline (PBS; without Ca^{2+} and without Mg^{2+}; Gibco), followed by treatment with Collagenase B (1 mg/ml) in low calcium solution (Maltsev et al., 1994; 120 mM NaCl; 5.4 mM KCl; 5 mM $MgSO_4$*7 H_2O; 5 mM Na-pyruvate; 20 mM glucose; 20 mM taurine; 10 mM HEPES/NaOH; and 30 µM (3 µg/ml) $CaCl_2$; pH: 6.9 at room temperature) for ∼30 min at 37°C by gentle agitation until a single-cell solution was obtained. Alternatively, CMs were dissociated with StemDiff Kit (5 min, 37°C, with mixing at 1,000 rpm; STEMCELL Technologies). Isolated cells were resuspended in IMDM Glutamax (Gibco, Thermo Fisher Scientific) supplemented with 10% fetal calf serum (FCS; GE Healthcare Life Science) and 10 µM Rho-associated protein kinase (ROCK)-inhibitor Y-27632 (Tocris). Resuspended CMs were plated onto laminin-coated (40 µg/ml; Life Technologies, Thermo Fisher Scientific) glass coverslips and cultivated for a further 35–69 d. After 1 d, the medium was changed to basic serum-free (bSF)-only medium, consisting of Dulbecco's modified Eagle's medium (DMEM; high glucose, pyruvate, no glutamine; Life Technologies, Thermo Fisher Scientific) supplemented with 2 mmol/liter *L*-glutamine, 1% nonessential amino acids (Gibco, Thermo Fisher Scientific), 100 U/ml penicillin-streptomycin (Gibco, Thermo Fisher Scientific), 0.1 mmol/liter β-mercaptoethanol, 17 µg/ml sodium selenite, 11 µg/ml transferrin, and 10 µg/ml human insulin (all Sigma-Aldrich, Merck), and changed twice a week. To enrich for CMs, a transgenic hES3 αMyHCneoPGKhygro line carrying a selection marker for Neomycin controlled by the CM-specific αMyHC-promotor was used (Schwanke et al., 2014). 200 µg/ml G418 (Gibco, Thermo Fisher Scientific) was added over the first 7 d of cultivation of hESC-CMs on laminin-coated glass coverslips to generate an essentially pure CM population. For replating, hESC-CMs were treated with 200 µl Collagenase B (1 mg/ml) in low calcium solution (Maltsev et al., 1994) per coverslip for 30 min at 37°C (days 42, 45, 48, and 55) or with 500 µl Accutase (Gibco, Thermo Fisher Scientific) per coverslip for 5 min at 37°C (days 34, 35, and 42). Dissociated hESC-CMs were reseeded on laminin-coated glass coverslips in IMDM Glutamax supplemented with 10% FCS and 10 µM ROCK-inhibitor Y-27632 for 23 h and further cultivated in bSF-only medium (Fig. 1).

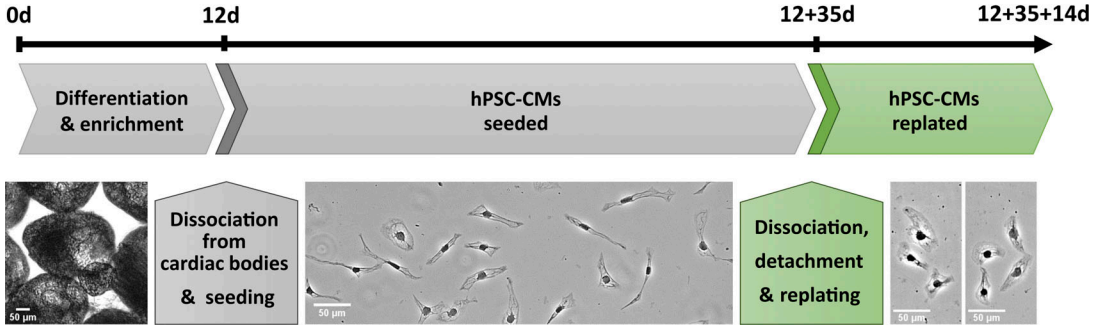

Figure 1. **Outline of differentiation, enrichment, seeding, and replating of hPSC-CMs on laminin-coated glass coverslips, a stiff matrix.** hPSC-CMs were differentiated, enriched, seeded, and replated on indicated days.

In pharmacological interference experiments, hESC-CMs grown on laminin-coated glass coverslips were treated from day 7 on for 2 or 4 d with or without 5 µM FAK-inhibitor 14 (Santa Cruz Biotechnology) dissolved in ethanol or DMSO, or with 10 µM MEK1/2 inhibitor U0126 (Cell Signaling) dissolved in DMSO from day 7 on for 2 d. Additionally, hESC-CMs grown on Matrigel-coated (Corning) polydimethylsiloxane (PDMS; Specialty Manufacturing, Inc.) coverslips were treated for 2 d until day 35 with or without 5 µM FAK inhibitor 14, or 10 µM MEK1/2 inhibitor U0126.

Differentiation and cultivation of hiPSC-CMs

Wild-type hiPSC-CMs Phoenix were cultivated and differentiated into CMs followed by purification using a modified protocol as previously described (Chatterjee et al., 2021; Haase et al., 2017; Kreutzer et al., 2022). Briefly, differentiation was initiated at 75–80% confluency with 5 µM CHIR99021 (Merck) in cardio differentiation medium (500 ml RPMI 1640 medium, GlutaMAX Supplement, HEPES [Life Technologies], 250 mg human recombinant albumin [Sigma-Aldrich], 100 mg *L*-ascorbic acid 2-phosphate sesquimagnesium salt hydrate [Sigma-Aldrich]) in 12-well plates (Greiner) coated with Geltrex (Invitrogen, Thermo Fisher Scientific). After 48 h, fresh medium with 5 µM IWP2 (Selleck) was added. The medium was exchanged every 48 h. At day 8 of differentiation, cells started to contract spontaneously. From this time point, cells were maintained in cardio culture medium (500 ml RPMI 1640 medium, GlutaMAX Supplement, HEPES [Life Technologies], 10 ml B-27 Supplement [50X], serum free [Life Technologies]) with the medium changed every 2 d. At day 15, cells were dissociated and seeded to T25 flasks (Corning). Briefly, cells were washed with Versene (Life Technologies, Thermo Fisher Scientific) and treated for 5 min at 37°C with 5X Trypsin-EDTA (Life Technologies, Thermo Fisher Scientific) in PBS. Cells were collected, centrifuged at 200 × *g* for 5 min at RT, and resuspended in cardio digestion medium (80 ml Cardio Culture Medium, 20 ml heat-inactivated FBS [Life Technologies, Thermo Fisher Scientific], 100 µl thiazovivin [Selleck]). Cells were seeded at a density of 500,000 cells per T25 flasks coated with 0.1% gelatin. After three days, medium was changed to cardio selection medium (500 ml RPMI 1640 [without glucose, without HEPES; Life Technologies, Thermo Fisher Scientific], 250 mg human recombinant albumin, 100 mg *L*-ascorbic acid 2-phosphate sesquimagnesium salt hydrate, 2 ml sodium DL-lactate solution [60%, wt/wt; Sigma-Aldrich] in HEPES [Sigma-Aldrich]) for 7 d to further enrich CMs. Then, medium was shifted back to cardio culture medium until day 46, when cells were dissociated again using the protocol as described above. For immunostaining, CMs were seeded in a density of 100,000 cells on 18-mm laminin-coated glass coverslips. For protein expression analysis, CMs were seeded at a density of 200,000 cells on 32-mm laminin-coated glass coverslips. Cells were cultivated in cardio culture medium until days 64 or 66. For replating, a fraction of 64-d (=18 d on laminin-coated glass coverslips)-old cells were treated for 5 min at 37°C with Trypsin-EDTA. Dissociated cells were subsequently replated on laminin-coated glass coverslips and kept for two more days in cardio digestion medium. On day 66, cells were lysed for protein expression analysis or fixated with 4% paraformaldehyde (Merck) for immunostaining (see below).

Immunofluorescence analysis of MyHC and MLC isoform expression

Immunostaining of single hESC-CMs with specific primary antibodies against α-MyHC (rabbit, polyclonal, α-huMYH6; BioGenes) and β-MyHC (mouse, monoclonal, M8421; Sigma-Aldrich, Merck), and secondary anti-rabbit Alexa Fluor 488 (goat, polyclonal, A11008; Thermo Fisher Scientific) for α-MyHC and anti-mouse Alexa Fluor 555 antibodies (goat, polyclonal, A21422; Thermo Fisher Scientific) for β-MyHC was performed as described previously (Weber et al., 2016, 2020). For myosin regulatory light chain (MLC2) isoforms, specific primary antibodies against MLC2a (mouse, monoclonal, 311 011; Synaptic Systems) and MLC2v (rabbit, polyclonal, 10906-1-AP; Proteintech), and secondary anti-mouse Alexa Fluor 555 (donkey, polyclonal, A31570; Thermo Fisher Scientific) for MLC2a and anti-rabbit Alexa Fluor 488 (donkey, polyclonal, A21206; Thermo Fisher Scientific) for MLC2v were used. DAPI (Sigma-Aldrich) was used as a nuclear counterstain. Dilutions of antibodies and staining duration were identical for each experiment. Imaging was done using either an Olympus IX51 fluorescence microscope (Olympus) with an Olympus LCAch N Phase 20×/0.40 NA Php or Olympus LCAch 40×/0.55 NA Php objective lens, and filter sets for DAPI (BP330-385, ET460/50M; Chroma), GFP (HQ470/40X, HQ525/50M; Chroma), and Cy3 (HQ546/11X,

HQ585/40M; Chroma), or an Olympus IX83 fluorescence microscope with an Olympus LUCPlanFL N 20×/0.45 NA or Olympus UPlanFl 40×/0.75 NA Ph2 objective lens and a cooled CCD camera (Orca-R²; Hamamatsu Photonics), using filter sets for DAPI (AT350/50X, ET460/50M, T400LP; Chroma), GFP (ET470/40X, ET525/50M, T495LPXR; Chroma), and Cy3 (ET545/25X, ET605/70M, T565LPXR; Chroma). Images of CMs were taken using identical exposure times for both α-MyHC and β-MyHC or MLC2a and MLC2v specific channels and saved in greyscale. Classification and scoring of myosin isoform expression of single CMs using the unmodified original image files was based on specific staining of sarcomeres only and performed as described previously (Weber et al., 2016, 2020).

For single-cell IF, the fractions of cells in the different categories were assigned as described previously (Weber et al., 2020).

Myosin isoforms

Red: β, exclusively β-MyHC expressing CMs; orange: β > α, coexpression of α- and β-MyHC with higher level of β-MyHC fluorescence; yellow: α = β, coexpression of α- and β-MyHC with equivalent fluorescence levels; α > β: light green, coexpression of α- and β-MyHC with higher level of α-MyHC fluorescence; green: α, exclusively α-MyHC expressing CMs.

MLC2 isoforms

Magenta: MLC2v, exclusively MLC2v expressing CMs; purple: v > a, coexpression of MLC2v and MLC2a with higher level of MLC2v fluorescence; dark blue: v = a, coexpression of MLC2v and MLC2a with equivalent fluorescence levels; a > v: light blue, coexpression of MLC2v and MLC2a with higher level of MLC2a fluorescence; cyan: MLC2a, exclusively MLC2a expressing CMs.

Protein expression analysis

For sarcomeric protein analysis, plated hPSC-CMs were lysed in kinase buffer (20 mM Tris-acetate, pH 7.0; 0.1 mM EDTA; 1 mM EGTA; 1 mM Na_3VO_4; 10 mM β-glycerolphosphate; 50 mM NaF; 5 mM pyrophosphate; 1% Triton X-100; 2 µg/ml leupeptin; and 0.27 M sucrose, supplemented with Protease Inhibitor Cocktail [Bimake] and Phosstop Phosphatase Inhibitor Cocktail [Roche]). For loading, lysates were mixed (4:1) with RotiLoad1, 4× conc. (Roth). As native tissue controls, adult human atrial and ventricular samples were prepared. SDS-PAGE gels for detection of MyHCs (8% SDS with 5% glycerol) were performed as described previously (Iorga et al., 2018; Kraft et al., 2013).

For the detection of (phospho-)FAK and (phospho-)ERK1/2, hESC-CM samples were prepared as described above. Following separation of proteins by SDS-PAGE (10% SDS gel), proteins were transferred onto a nitrocellulose blotting membrane (0.22 µm) and blocked in 5% milk powder (Santa Cruz) dissolved in Tris-buffered saline (TBS) with 0.1% Tween 20 (TBS-T; Sigma-Aldrich). Primary antibodies against FAK (mouse, monoclonal, sc-271126; Santa Cruz), phospho-FAK (rabbit, polyclonal, 3283; Cell Signaling), ERK1/2 (rabbit, polyclonal, 9102; Cell Signaling), phospho-ERK1/2 (rabbit, polyclonal, 9101; Cell Signaling), or β-tubulin (mouse, monoclonal, G098; Applied Biological Materials Inc.) were incubated in TBS-T at 4°C overnight. Secondary antibodies against mouse (from goat, 1721011; Bio-Rad) or rabbit (from goat, 1706515; Bio-Rad) were incubated in TBS-T for 1 h at RT. Western blot image acquisition was done using enhanced chemiluminescence with an ImageQuant LAS 4000 imaging system (GE Healthcare).

Assessment of the contractile function of subcellular myofibrils

Following the chemical demembranation of replated (2, 3, 6, 7, 8, 9, and 10 d) or non-replated (35 d) hESC-CMs, intracellular myofibrils became accessible and, therefore, a thin myofibrillar bundle was attached between a stiff needle and an nN-sensitive force probe in a myofibrils micromechanical setup, as described previously (Iorga et al., 2018). While myofibrils were exposed to an EGTA-relaxing solution (free of Ca^{2+}), their sarcomere lengths (SL) were adjusted to SL = 2.3 µm for determining a sarcomeric passive force (F_{pass}) mainly due to stretching titin filaments. Then, isometrically kept myofibrils were Ca^{2+}-activated with a solution containing saturating [Ca^{2+}] (pCa 4.18) and started to develop force with the rate constant k_{act} (Fig. 2 A).

When the force reached a maximum and steady-state value, a quick (30 ms) release–restretch maneuver (Brenner's maneuver; Brenner, 1988) leading to transient decrease and subsequent redevelopment of force was performed. The total force magnitude F_{total} can thus be measured. This maneuver allows the determination of the active force ($F_{act} = F_{total} - F_{pass}$; Fig. 2 A) due to cycling myosin–actin crossbridges when thin filaments are turned-on upon Ca^{2+} activation. During this maneuver, the isometric condition is shortly broken and most crossbridges populate transiently non-force-generating states (i.e., force drops near zero; Fig. 2 A). Considering a two-state model (Brenner, 1988), crossbridges redistribute with the rate constant k_{tr} between non-force- and force-generating states after this transient isometric–isotonic–isometric perturbation. The rate constant k_{tr} is determined by f_{app} (rate constant or probability of crossbridges entering force-generating states) and by g_{app} (rate constant or probability of crossbridges leaving force-generating states) that both depends strongly on the MyHC isoform (Locher et al., 2009). f_{app} depends on thin filament state (i.e., it depends on [Ca^{2+}]), while g_{app} is independent of [Ca^{2+}]. Therefore, Ca^{2+} modulates k_{tr} (= f_{app} + g_{app}) and F_{act} (~f_{app}/(f_{app} + g_{app}); Iorga et al., 2018).

Upon rapid removal of Ca^{2+}, myofibrils relax in a biphasic manner. During the first relaxation phase, force decays slowly, almost linearly with the rate constant k_{lin}, while sarcomeres maintain their short length (Iorga et al., 2018). The rate constant k_{lin} of this sarcomeric isometric phase represents g_{app} that depends on the tension cost (myosin ATPase/force; Iorga et al., 2018; Weber et al., 2020).

During the second relaxation phase, force decays faster than during the first relaxation phase with the rate constant k_{rel}, during which sarcomeres elongate sequentially along the myofibrils, reducing thus the mechanical stress to which crossbridges were subjected as compared with the first, isometric relaxation phase, or during Ca^{2+}-activation force plateau (Iorga et al., 2018). The amplitude of force decay of the second relaxation phase is much larger than that of the first phase

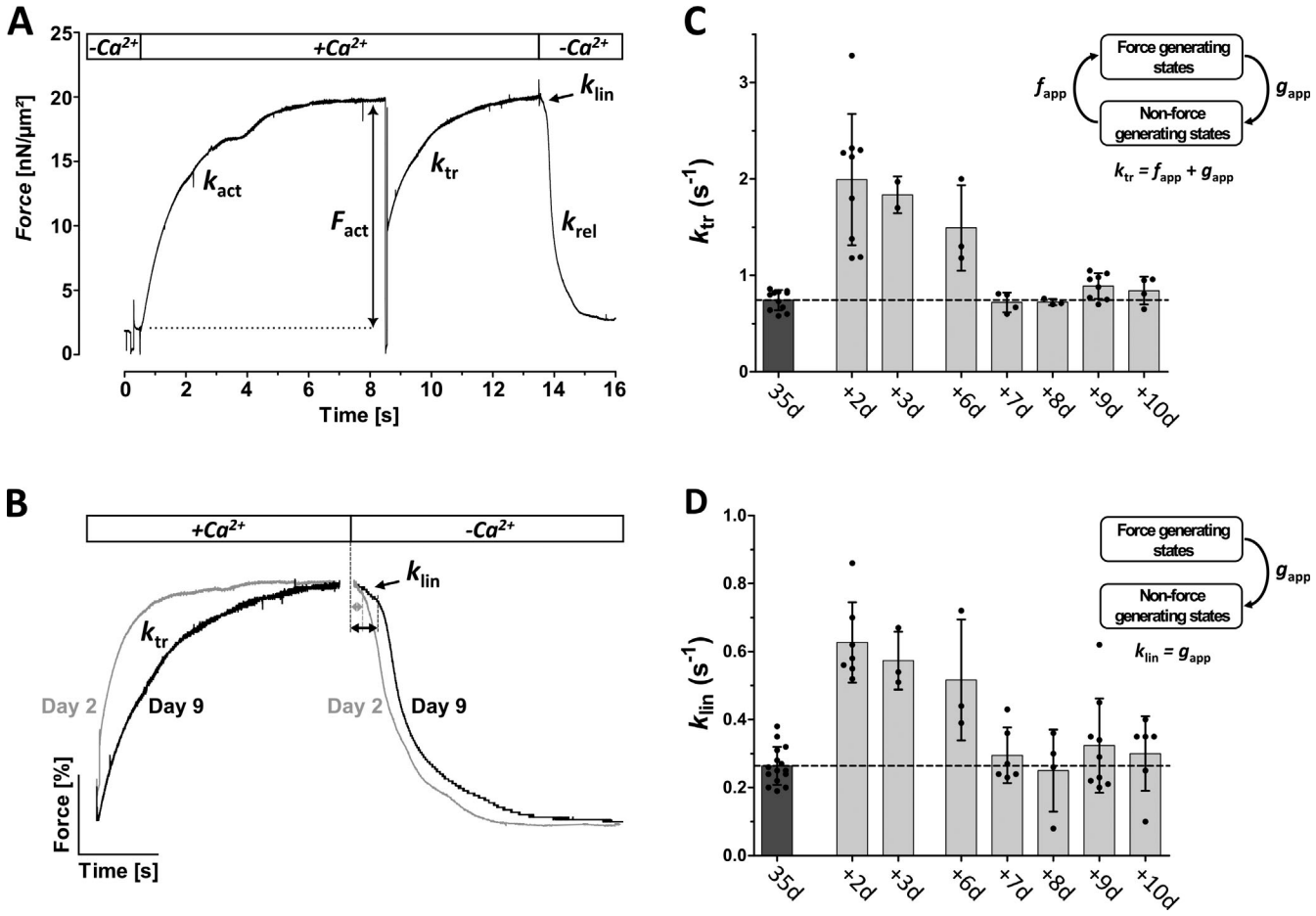

Figure 2. **Analysis of force-related kinetic parameters of myofibrils from demembranated replated hESC-CMs. (A)** Example of a force trace indicating the protocol (on top) of sarcomeric activation (+Ca^{2+}) and relaxation (–Ca^{2+}) and the force-related parameters: rate constant of Ca^{2+}-induced force development (k_{act}), amplitude of the isometric force generated by cycling crossbridges (F_{act}), rate constant of mechanically induced force redevelopment of Ca^{2+}-activated myofibrils (k_{tr}), rate constant of the linear force decay during the first, slow phase of relaxation (k_{lin}), and the rate constant of the monoexponential force decay during the second, fast phase of relaxation (k_{rel}). **(B)** Force traces during force redevelopment and relaxation for myofibrils of hESC-CMs replated for 2 (grey) or 9 (black) days. Small horizontal arrows indicate the duration of the first relaxation phase (t_{lin}) on days 2 and 9. **(C and D)** k_{tr}, reflecting crossbridge cycling kinetics (C), and k_{lin} (D), reflecting crossbridges leaving force-generating states in replated hESC-CMs on indicated days, and in 35 d old non-replated hESC-CMs (data imported from Iorga et al. [2018]). Mean ± SD; n = 2–20 myofibrillar bundles obtained from 12 coverslips derived from one differentiation. Insets: Diagrams representing the two states of cycling cross-bridges. f_{app}: rate constant or probability of cross-bridges entering force-generating states); g_{app}: rate constant or probability of cross-bridges leaving force-generating states.

(Fig. 2, A and B). The rate constant k_{rel} of the second relaxation phase reflects remaining crossbridges, leaving force-generating states under a reduced mechanical load with a higher probability than g_{app}.

Analysis of intracellular calcium transients

Intracellular calcium transients of single CMs were recorded using a dual excitation fluorescence photomultiplier system (IonOptix Corp.) as described previously (Weber et al., 2020). Briefly, for recordings of intracellular calcium transients of hESC-CMs cultivated for 35 d and those additionally cultivated for 1–4 d after replating, coverslips with adherent CMs were loaded with the ratiometric indicator Fura-2 AM18 (Thermo Fisher Scientific) for 25 min and rinsed twice with DMEM for 15 min. Then they were placed in a homemade perfusion chamber and paced by electrical stimulation at 1 Hz (25 V, 4 ms at 37 ± 0.5°C). After alternating excitation with 340 and 380 nm, emission was recorded at 510 nm. Autofluorescence was measured from 10 unloaded CMs from the same batch and subtracted from recordings before calculating the fluorescence ratio (340/380 nm). Time to peak, half-decay time, calcium amplitude, and calcium rise velocity were determined using IonWizard software (IonOptix Corp.).

Total RNA isolation

Total RNA was isolated from hESC-CMs and hiPSC-CMs cultivated for 37 d or replated on day 35 and cultivated for 2 more days using the peqGOLD Total RNA Kit (Peqlab; VWR Life Science; Avantor), according to the manufacturer's instructions.

Library generation, sequencing, and raw data processing

Library generation, quality control, and quantification

70 ng of total RNA per sample were utilized as input for mRNA enrichment procedure with NEBNext Poly(A) mRNA Magnetic

Isolation Module (E7490L; New England Biolabs) followed by stranded cDNA library generation using NEBNext Ultra II Directional RNA Library Prep Kit for Illumina (E7760L; New England Biolabs). All steps were performed as recommended in user manual E7760 (version 1.0_02-2017; New England Biolabs), except that all reactions were downscaled to 2/3 of initial volumes. Furthermore, one additional purification step was introduced at the end of the standard procedure using 1× Agencourt AMPure XP Beads (#A63881; Beckman Coulter, Inc.).

cDNA libraries were barcoded by a dual indexing approach using NEBNext Multiplex Oligos for Illumina—96 Unique Dual Index Primer Pairs (6440S; New England Biolabs). All generated cDNA libraries were amplified with 11 cycles of final PCR.

Fragment length distribution of individual libraries was monitored using Bioanalyzer High Sensitivity DNA Assay (5067-4626; Agilent Technologies). Quantification of libraries was performed by use of the Qubit dsDNA HS Assay Kit (Q32854; Thermo Fisher Scientific).

Library denaturation and sequencing run

Equal molar amounts of 10 individually barcoded libraries were pooled. Accordingly, each analyzed library constitutes 10% of overall flowcell/run capacity. The library pool was denatured with NaOH and finally diluted to 2 pM according to the Denature and Dilute Libraries Guide (document# 15048776 v02; Illumina). 1.3 ml of the denatured pool was loaded to an Illumina NextSeq 550 sequencer using a High Output Flowcell for single reads (20024906; Illumina). Sequencing was performed with the following settings: sequence reads 1 and 2 with 38 bases each; index reads 1 and 2 with 8 bases each.

BCL to FASTQ conversion

BCL files were converted to FASTQ files using bcl2fastq conversion software version v2.20.0.422 (Illumina).

Raw data processing and quality control

Raw data processing was conducted by use of nfcore/rnaseq (version 1.4.2), which is a bioinformatics best-practice analysis pipeline used for RNA sequencing data at the National Genomics Infrastructure at SciLifeLab, Stockholm, Sweden. The pipeline uses Nextflow, a bioinformatics workflow tool. It preprocesses raw data from FASTQ inputs, aligns the reads, and performs extensive quality control on the results. The genome reference and annotation data were taken from https://www.gencodegenes.org/human/release_34.html (*Homo sapiens*; GRCh38.p13; release 34).

Normalization and differential expression analysis

Normalization and differential expression analysis were performed with DESeq2 (Galaxy Tool Version 2.11.40.2) with default settings except for "Output normalized counts table," "Turn off outliers filtering," and "Turn off independent filtering," all of which were set to "True."

Data deposition

Datasets associated with this article can be downloaded from GEO (accession no. GSE176154).

Statistical analysis

Results are presented as mean ± SEM (SDS-PAGE and Western blot analysis) or mean ± SD (force-related parameters, calcium transient parameters, IF analysis). Differences between replated and non-replated hPSC-CMs or between treated and untreated hESC-CMs were either analyzed by unpaired Student's *t* test (force-related parameters, protein expression analysis) or Mann-Whitney U-test (calcium transient parameters). A nested *t*-test was applied to account for multiple differentiations of hPSC-CMs in experiments related to Fig. 3 and Fig. 4 C. Significant differences were indicated as $P < 0.05$ (*), $P < 0.01$ (**), or $P < 0.001$ (***). Statistical analyses were performed using GraphPad Prism 9.5.1.

Ethics statement

The ethics committee of Hannover Medical School approved the studies with anonymized human tissue and experiments were carried out in accordance with the given recommendations (no. 2276-2014). Written informed consent according to the World Medical Association (2013) was given by all subjects.

Results

Alterations of contractile function in replated hESC-CMs

To investigate the potential effect of detachment from the stiff substrate and subsequent replating of long-term plated hESC-CM on contractile function, we determined functional parameters of subcellular myofibrils from chemically demembranated hESC-CMs. For this purpose, hESC-CMs were enzymatically detached from and then replated on laminin-coated coverslips, and force-related kinetics of isometrically held myofibrils were measured from days 2–10 after replating (Fig. 2, A–D; and Table 1). Experiments were performed at saturating [Ca^{2+}] with the purpose to minimize the potential differences due to Ca^{2+}-regulation at intermediate [Ca^{2+}] between myofibrils of replated and non-replated hESC-CMs. When Ca^{2+}-activated, replated hESC-CMs generated a smaller maximum isometric force (F_{act}) normalized to the cross-section of the myofibrillar bundle compared with control, non-replated hESC-CMs (Table 1).

When fully Ca^{2+}-activated (pCa 4.18), the rate constant of force development k_{act} was significantly increased on day 2 as compared with non-replated, exclusively β-MyHC-expressing hESC-CMs (Iorga et al., 2018; Table 1). Following a quick release–restretch maneuver, the rate constant of force redevelopment (k_{tr}) and the rate constant of slow force decay (k_{lin}) during the first relaxation phase following Ca^{2+} removal were also both significantly increased on day 2 (Fig. 2, C and D; and Table 1) as compared with non-replated, exclusively β-MyHC-expressing hESC-CMs (Iorga et al., 2018). The k_{tr} value on day 2 of replated hESC-CMs (2.01 ± 0.64 s^{-1}) approached the k_{tr} of exclusively α-MyHC-expressing hESC-CMs (2.44 ± 0.30 s^{-1}; Weber et al., 2016). The duration of the first relaxation phase was slightly shorter (smaller t_{lin}) in myofibrils from replated hESC-CMs on days 2–6 than on days 7–10 or as compared to non-replated cells (Fig. 2 B and Table 1). Mean values of the rate constant k_{rel} were similar for myofibrils of all investigated cells

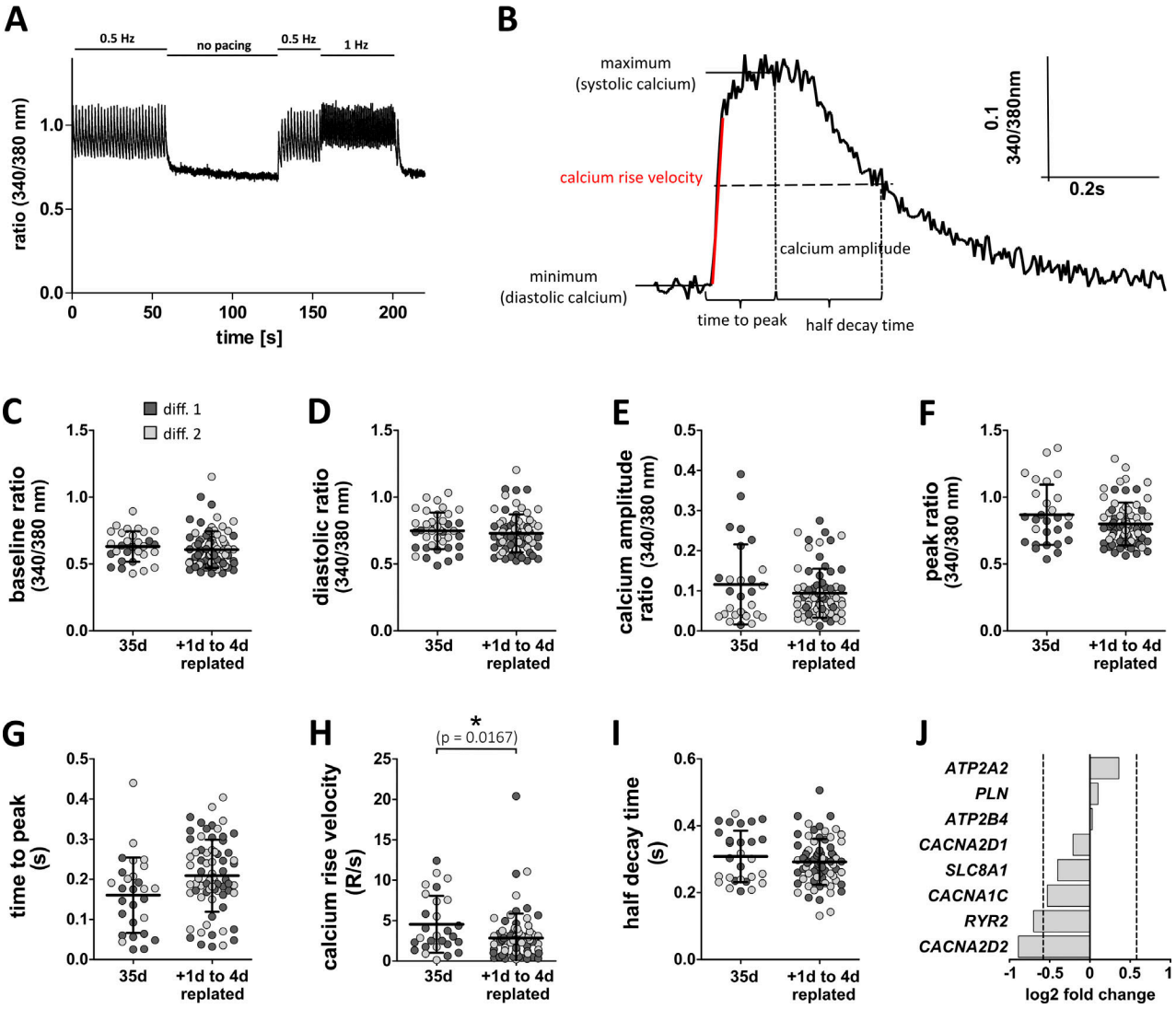

Figure 3. **Calcium transients from hESC-CMs replated for 1 to 4 d from day 35 onward without electrical pacing and then paced with 1 Hz. (A)** Representative electrical stimulation protocol. Stimulation with 0.5 Hz for 1 min, followed by a stimulation break for registration of basal ratio (basal calcium). The basal ratio was measured at the end of the break where ratio reached a stable phase. Then, the frequency was increased from 0.5 to 1 Hz for ∼1 min. Calcium transients were analyzed during 1 Hz stimulation. **(B)** Representative averaged calcium transient with analyzed parameters of minimum (diastolic), maximum (systolic, peak ratio) 340/380 nm ratios, calcium amplitude (difference between maximum and minimum 340/380 nm ratios), time to peak, half decay time, and maximum calcium rise velocity (red). Parameters were calculated after fitting the averaged calcium transients using IonWizard software. **(C–I)** Baseline calcium level (C) without electrical stimulus (baseline ratio 340/380 nm), (D) diastolic (minimum) calcium level (diastolic ratio 340/380 nm), (E) calcium amplitude (ratio 340/380 nm), (F) peak ratio (peak ratio 340/380 nm, maximum calcium level), (G) time to peak (in s), (H) calcium rise velocity (R/s; R: ratio 340/380 nm), and (I) half-decay time of calcium transients (in s). Calcium transients were determined under electrical stimulation with 1 Hz using the ratiometric calcium indicator Fura-2 and compared with non-replated hESC-CMs. Ratio: emission at 510 nm measured after alternating excitation at 340 nm/380 nm. Mean ± SD; n = 28–71 cells from 5–20 individual coverslips derived from two differentiations. Cells are colored according to the hESC-CM differentiation they were derived from (dark grey: differentiation no. 1; light grey: differentiation no. 2). *, P < 0.05. **(J)** hESC-CMs grown for 35 d on laminin-coated glass coverslips were detached, replated, cultivated for two additional days, and compared with 37-d-old non-replated cells; n = 3. mRNA expression for indicated genes of calcium handling was analyzed by RNA-seq. Data are presented as log2 fold change. The dashed line at ±0.585 indicates a ±1.5-fold change.

(Table 1). Changes in the kinetic parameters on days 2–6 were reversed in the second week after replating (Fig. 2, C and D; and Table 1). Taken together, the data indicate alterations of myofibrillar force-related kinetic parameters reflecting crossbridge cycling in sarcomeres of replated hESC-CMs for up to 6 d after replating, which were completely reversed in the second week after replating (Table 1).

According to the two-state crossbridge model (Brenner, 1988; Iorga et al., 2018), k_{tr} and k_{lin} directly allow us to determine the rate constants (or probabilities) of crossbridges entering (f_{app}) and leaving (g_{app}) force-generating states (Fig. 2, C and D). In hESC-CMs replated for 2 d, f_{app} and g_{app} increased significantly compared with 35 d old non-replated cells (Table 2), while f_{app} and g_{app} from hESC-CMs replated for 9 d were not significantly

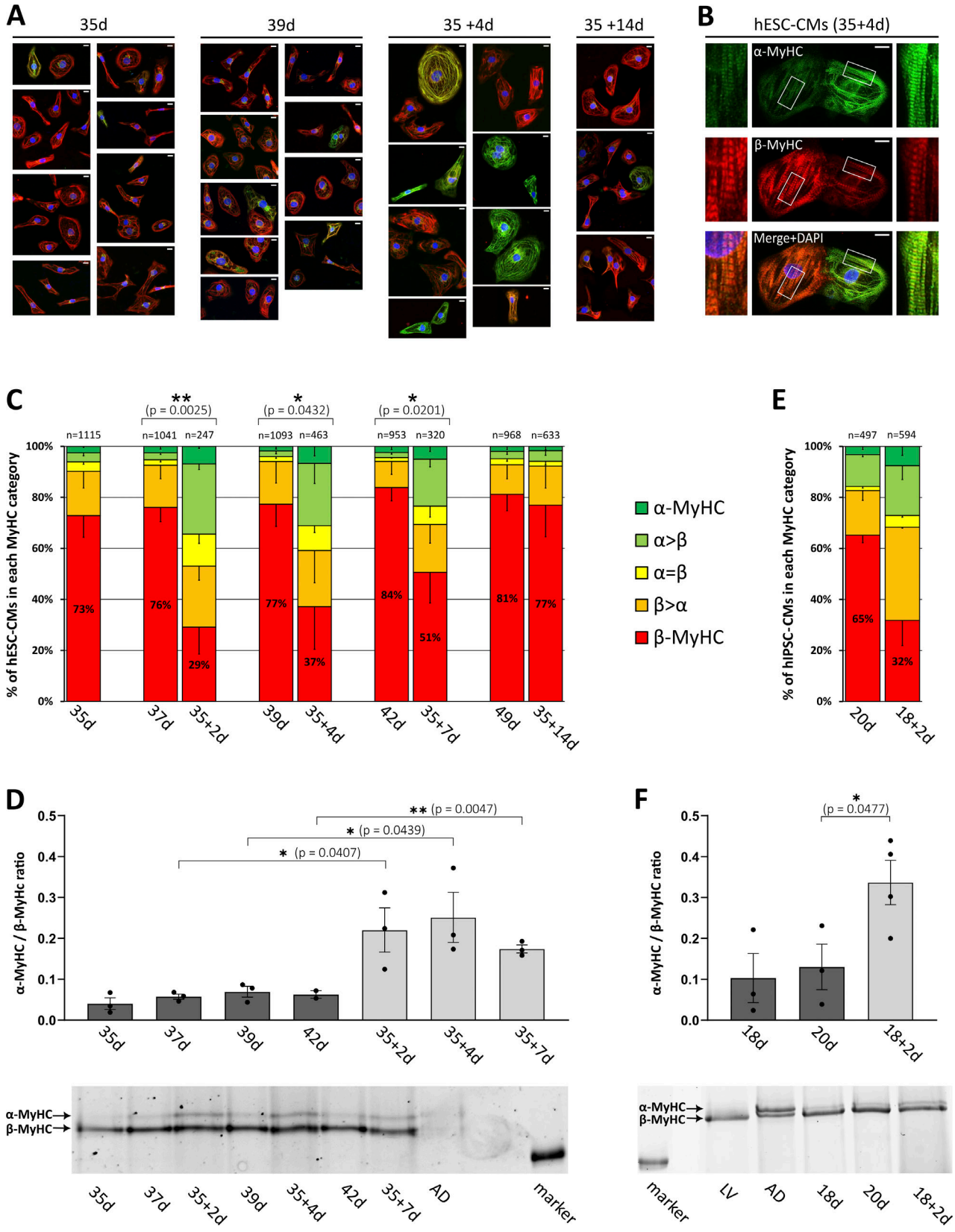

Figure 4. **Analysis of myosin isoform expression in replated hPSC-CMs.** hESC-CMs or hiPSC-CMs were cultivated for indicated days on laminin-coated glass coverslips or replated on day 35 or day 18, respectively, and further cultivated for indicated days. **(A)** Myosin isoform expression was analyzed in hESC-CMs by single-cell immunofluorescence (IF) using specific antibodies against α- (green) and β-MyHC (red). Nuclei were stained with DAPI (blue). Scale bars: 10 µm. **(B)** Single-cell IF analysis showing replated hESC-CMs from 35 + 4 d with mixed α- and β-MyHC expression with insets (white squares) demonstrating a detailed view of sarcomeric staining as relevant for classification (see below). Scale bars: 10 µm. **(C)** Single-cell IF analysis of myosin expression in hESC-CMs.

The fractions of cells in the different categories (see Materials and methods) are shown as the percentage of the total number of cells analyzed (*n*, set to 100%) for each time point. Mean ± SD; indicated number of cells (*n*) were obtained from six individual coverslips derived from three differentiations; P values: exclusively β-MyHC expressing cells. **(D)** MyHC isoforms were separated by SDS-PAGE and the ratio of α-MyHC/β-MyHC expression in hESC-CMs was determined densitometrically. Mean ± SEM; *n* = 3 individual coverslips from three differentiations. Representative SDS-PAGE gel with samples from human right atrium (AD) as indicated; molecular weight marker: 200 kD. **(E)** Myosin isoform expression was analyzed in hiPSC-CMs by single-cell IF using specific antibodies against α- and β-MyHC. The fractions of cells in the different categories (see Materials and methods) are shown as a percentage of the total number of cells analyzed (*n*, set to 100%) for each time point. Mean; two coverslips derived from one differentiation. **(F)** MyHC isoforms were separated by SDS-PAGE and the ratio of α-MyHC/β-MyHC expression in hiPSC-CMs was determined densitometrically. Mean ± SEM; *n* = 3 or 4 individual coverslips from one differentiation. Representative SDS-PAGE gel, with samples from the human right atrium (AD) and left ventricle (LV) as indicated; molecular weight marker: 200 kD. Source data are available for this figure: SourceData F4.

changed (Table 2), thus indicating reversibility of observed changes.

Changes in calcium transients in replated hESC-CMs

Further, we measured intracellular calcium transients of intact, single hESC-CMs after loading with the ratiometric calcium indicator Fura-2 (Fig. 3, A and B). The baseline calcium level was not different between replated and long-plated hESC-CMs without electrical stimulation (Fig. 3 C). Minimum (diastolic) calcium level, calcium amplitude, and maximum (systolic, peak) calcium level (peak ratio) of hESC-CMs electrically stimulated at a frequency of 1 Hz were not changed compared with non-replated cells (Fig. 3, D–F). While time to peak was not altered significantly, maximum calcium rise velocity was slower (Fig. 3, G and H) in replated compared with non-replated hESC-CMs. Half decay time of calcium transients was not changed (Fig. 3 I).

RNA-sequencing (RNA-Seq) demonstrated reduced mRNA expression levels of *CACNA1C*, *CACNA2D2*, and *RYR2*, genes encoding for proteins of calcium-handling, in hESC-CMs replated for 2 d as compared with 37-d-old controls (Fig. 3 J), which is consistent with the observed slower kinetics of calcium transients in replated CMs.

Increased expression of α-MyHC in replated hESC- and hiPSC-CMs

The rate constants of force-generating crossbridge states that we found to be changed in replated hESC-CMs (Table 2) depend on MyHC isoform expression (Locher et al., 2009). Therefore, to assess the expression of α-/β-MyHC isoforms, we performed single-cell immunofluorescence (IF) analysis with hESC-CMs detached and replated on day 35 of culture. One day after replating, sarcomeric structures were not easy to discern (data not shown) but became apparent on day 2. Single-cell IF analysis showed a robust increase in exclusively α-MyHC and mixed α/β-MyHC expression in replated hESC-CMs on days 2, 4, and 7 (Fig. 4, A–C), leading to a profound increase in heterogeneity of MyHC isoform expression among CMs compared with non-replated controls. Interestingly, the level of exclusively β-MyHC expressing replated hESC-CMs increased again over time and was comparable with non-replated controls after 14 d. SDS-PAGE analysis confirmed increased expression of α-MyHC in replated hESC-CMs compared with non-replated CMs (Fig. 4 D and Table 3). Replating of hiPSC-CMs also induced a comparable shift from mainly β-MyHC expressing cells to more exclusive α-MyHC and heterogeneous α-/β-MyHC expression (Fig. 4, E and F; and Table 3), indicating that the observed effects are not only specific to CMs derived from hESCs.

Furthermore, increased expression of exclusively α-MyHC and mixed α/β-MyHC also occurred when hESC-CMs were detached and replated after extended long-term cultivation on a stiff matrix on days 42, 45, 48, and 55, compared with day 34 (Fig. 5, A–E), with the restitution of the predominance of exclusively β-MyHC expressing hESC-CMs after 2 wk showing a certain degree of variation.

We further analyzed the mRNA expression profile of genes encoding for sarcomeric proteins that have been shown to affect myofibrillar contractile function (Iorga et al., 2018) by RNA-Seq. *MYH6* mRNA expression of hESC-CMs replated for 2 d was profoundly upregulated (fold change 3.52; Fig. 5 F and Table 4) compared with non-replated cells, while the mRNA expression of *MYH7* (fold change −1.59; Fig. 5 F and Table 4) was less affected, resulting in a nearly equal level of *MYH6* and *MYH7*

Table 1. **Force-related steady-state and kinetic parameters of myofibrils from replated hESC-CMs**

Force-related parameters	35 d	+2 d	+3 d	+6 d	+7 d	+8 d	+9 d	+10 d
F_{act} (kPa)	42 ± 10	32 ± 11	26 ± 11	24 ± 2[a]	22 ± 9[a]	18 ± 6[a]	25 ± 10[a]	22 ± 10[a]
k_{act} (s^{-1})	0.66 ± 0.14	1.56 ± 0.33[a]	1.64 ± 0.48	1.26 ± 0.27	0.75 ± 0.12	0.64 ± 0.02	0.69 ± 0.05	0.64 ± 0.02
k_{tr} (s^{-1})	0.75 ± 0.10	2.01 ± 0.64[a]	1.84 ± 0.19	1.49 ± 0.44	0.72 ± 0.10	0.72 ± 0.03	0.88 ± 0.12	0.84 ± 0.15
k_{lin} (s^{-1})	0.26 ± 0.06	0.64 ± 0.11[a]	0.57 ± 0.09[a]	0.52 ± 0.18	0.30 ± 0.08	0.25 ± 0.12	0.33 ± 0.13	0.30 ± 0.11
t_{lin} (ms)	197 ± 60	165 ± 61	134 ± 45	156 ± 51	191 ± 77	195 ± 92	199 ± 42	212 ± 46
k_{rel} (s^{-1})	4.62 ± 0.60	4.69 ± 2.15	3.93 ± 0.04	4.80 ± 0.79	4.02 ± 1.16	4.10 ± 0.91	4.33 ± 2.28	4.43 ± 0.96

Force-related steady-state (F_{act}) and kinetic parameters (k_{act}, k_{tr}, k_{lin}, t_{lin}, k_{rel}) of myofibrils from hESC-CMs replated for indicated days, and of non-replated (35 d) hESC-CMs (data imported from Iorga et al. [2018]). Data for most relevant cross-bridge-related parameters k_{tr} and k_{lin} are also shown in Fig. 2, C and D.
[a]Significance level at least P < 0.05 or smaller.

Table 2. **Kinetic parameters reflecting probabilities of crossbridges to enter and leave force-generating states of replated hESC-CMs**

Cross-bridge related parameters	Replated hESC-CMs		Non-replated
	2 d	9 d	35 d hESC-CMs
f_{app}	1.32 ± 0.75**	0.56 ± 0.16^{ns}	0.47 ± 0.11
g_{app}	0.64 ± 0.11**	0.33 ± 0.13^{ns}	0.26 ± 0.06

Kinetic parameters reflecting probabilities of crossbridges to enter (f_{app}) and leave (g_{app}) force-generating states of replated cells on indicated days, and of non-replated 35 d hESC-CMs with predominant exclusive β-MyHC expression (data imported from Iorga et al. [2018]). Data were calculated as indicated in Fig. 2, C and D. Mean ± SD; **, P < 0.01; ns, not significant, P > 0.05).

mRNA in replated hESC-CMs. The expression of genes of isoforms of myosin light chains and troponins was also less affected (Fig. 5 F). To conclude, MyHC isoform expression analysis demonstrated that detachment and subsequent replating of long-term plated hPSC-CMs led to a rapid increase of α-MyHC expression that could explain the observed changes in myofibrillar force-related kinetic parameters.

Gene enrichment analysis indicates changes in mechanosensation/-transduction

Gene enrichment analysis based on RNA-Seq data of hESC-CMs replated for 2 d after 35 d of cultivation as compared with 37 d old non-replated controls was performed by using the functional enrichment analysis web tool WebGestalt (WEB-based Gene SeT AnaLysis Toolkit; Liao et al., 2019). Gene ontology (GO) analysis of upregulated genes (fold change cutoff 1.5) showed significantly enriched biological process categories related to ECM and cell adhesion (Fig. 6 A), as well as to muscle development and function (Fig. 6 B). This emphasizes the impact of matrix stiffness change on cardiomyocyte interaction with a reorganized ECM and on cardiomyocyte function at the level of gene expression. Enrichment of categories like "response to mechanical stimulus" and "integrin-mediated signaling pathway" (Fig. 6 A) indicated the relevance of mechanosensation/-transduction for stiff matrix-induced changes in gene expression. In accordance, Ingenuity Pathway Analysis (IPA; Qiagen) demonstrated significant enrichment of pathways involved in mechanosensation/-transduction in cardiomyocyte response to mechanical stretch (Dostal et al., 2014; Sadoshima and Izumo, 1997), predominantly integrin- and, to a lesser extent, G-protein-associated pathways, while only a few calcium-associated pathways were enriched (Fig. 6 C). Taken together, in line with a change of matrix stiffness during dissociation and replating of the hESC-CMs, several categories enriched in GO analysis and IPA are related to ECM organization and cell interaction as well as to mechanosensation/-transduction with a focus on integrin-associated signaling.

β-MyHC expression is reduced by inhibition of FAK

To further investigate the possible impact of integrin-dependent signaling on MyHC-isoform expression, we analyzed the expression and phosphorylation level of FAK and its downstream mediator ERK1/2 in hESC-CMs. Western blot analysis demonstrated both expression and phosphorylation, indicating activation of FAK and ERK1/2 in hESC-CMs on days 7–35 (Fig. 7 A). Inhibition of FAK by FAK inhibitor 14 (5 μM) did not affect the ratio of phospho-ERK1/2/total ERK1/2, indicating that ERK1/2-phosphorylation appears to be mostly independent of FAK activation in 35-d-old hESC-CMs (Fig. 7 B).

IF analysis demonstrated a reduction of exclusively β-MyHC expression in hESC-CMs treated for 2 or 4 d with 5 μM FAK inhibitor 14, while 10 μM U0126, an inhibitor of ERK1/2 direct upstream kinase MEK1/2, had no significant effect (Fig. 7 C). The data indicate that β-MyHC expression is positively regulated by FAK but independent of MEK1/2–ERK1/2 signaling. In contrast to β-MyHC expression (see Fig. 4), only a minority of 35-d-old hESC-CMs grown on laminin-coated glass coverslips exclusively express the ventricular MLC isoform 2v, indicating a differential effect of stiff matrix on ventricular MyHC and MLC2 isoform expression (Fig. 7 D). The proportion of exclusively MLC2v and of all MLC2v expressing hESC-CMs was increased on a softer matrix, Matrigel-coated polydimethylsiloxane (PDMS). MLC2v expression was neither affected by 5 μM FAK inhibitor 14 nor by 10 μM of U0126 (Fig. 7 D), in addition, indicating differential regulation of isoform expression between MyHC and MLC2 in hESC-CMs.

Discussion

The presented work demonstrates a rapid increase of α-MyHC expression and its effects on calcium transients and myofibrillar contractile function in hESC-CMs that were long-term-cultured on a stiff matrix, detached, and subsequently replated.

Table 3. **Relative α-MyHC protein expression in replated hPSC-CMs**

	hESC-CMs									hiPSC-CMs	
α-MyHC	35 d	37 d	35 + 2 d	39 d	35 + 4 d	42 d	35 + 7 d	49 d	35 + 14 d	20 d	18 + 2 d
Mean (%)	3.86	5.46	17.73	6.48	19.72	5.92	14.83	8.61	5.32	11.12	24.82
± SD (%)	2.27	0.98	6.38	2.02	6.52	1.15	1.26	6.37	1.93	7.51	6.26

α-MyHC protein expression relative to total MyHC isoform protein expression (in percent) of replated and non-replated hESC- and hiPSC-CMs on indicated days. MyHC isoforms were separated by SDS-PAGE and MyHC isoform expression was determined densitometrically (see Fig. 4, D and F). Mean, hESC-CMs: n = 3 culture dishes from three differentiations; hiPSC-CMs: n = 3 or 4 culture dishes from one differentiation.

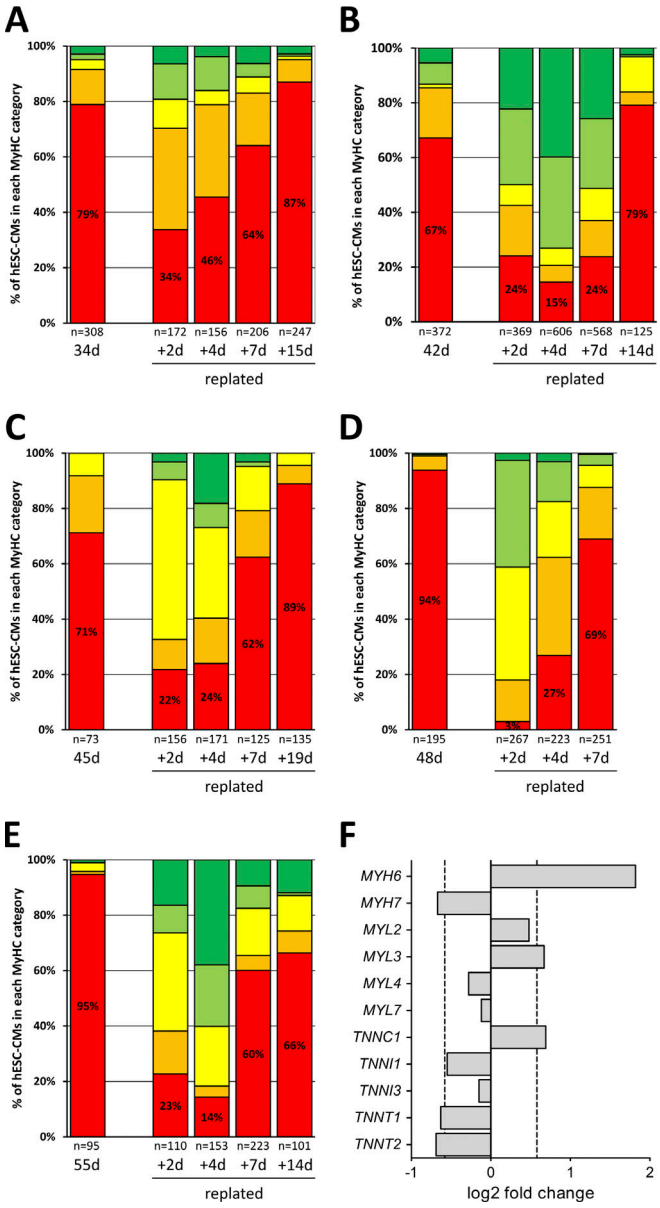

Figure 5. **IF analysis of myosin isoform expression in single hESC-CMs replated at different times. (A–E)** hESC-CMs grown for (A) 34, (B) 42, (C) 45, (D) 48, and (E) 55 d on laminin-coated glass coverslips were detached, replated on laminin-coated glass coverslips, grown for the indicated number of days (+d), and compared with non-replated controls (d). Myosin isoform expression was analyzed by single-cell IF using specific antibodies against α- and β-MyHC. The fractions of cells in the different categories are shown as a percentage of the total number of cells analyzed (*n*, set to 100%) for each time point (see Materials and methods). One coverslip from one differentiation each. **(F)** Changes in sarcomeric gene expression (log2 fold change) of hESC-CMs after replating compared with 37 d old non-replated controls. hESC-CMs grown for 35 d on laminin-coated glass coverslips were detached, replated on laminin-coated glass coverslips and cultivated for two more days. mRNA expression was analyzed using RNA-Seq data. Changes in mRNA expression of indicated myosin heavy chain (*MYH*), myosin light chain (*MYL*), and troponin (*TNN*) isoform genes are presented as log2 fold change. The dashed line at ±0.585 indicates a ±1.5-fold change; *n* = 3 culture dishes from three differentiations.

Table 4. ***MYH* isoform mRNA expression in replated hESC-CMs**

	Base mean			
Gene name	**37 d**	**35 + 2 d**	**log2(FC)**	**P-adj**
MYH6	20,165	107,324	1.82	4.52×10^{-7}
MYH7	201,052	106,418	−0.67	3.49×10^{-1}

MYH6 and *MYH7* mRNA base means in replated (35 + 2 d) vs. non-replated control (37 d) hESC-CMs derived from RNA-Seq. Base means, log2 fold change (log2(FC)), and adjusted P value (P-adj) from *n* = 3 culture dishes from three differentiations. Normalization and differential expression analysis was performed with DESeq2.

Significant differences in rate constants in replated compared with non-replated cells likely reflect the observed changes in the MyHC isoform composition that affect crossbridge turnover kinetics (Locher et al., 2009). The presented data suggest that within the first days (up to 1 wk) following replating, cross-bridge kinetics in replated hESC-CMs were faster, most likely due to an augmented ATPase activity related to re-expression of the α-MyHC isoform. Observed higher values for g_{app} in replated hESC-CMs indicate an elevated probability of cross-bridges entering non-force-generating states and suggest that replated cells would have an increased tension cost, a possibility that is supported by a reduced isometric force. Therefore, the re-expression of α-MyHC may impair the cellular energetics at the sarcomeric level.

Changes in force-related kinetic parameters in replated hESC-CMs expressing significant amounts of α-MyHC in contrast to non-replated long-term cultivated hESC-CMs are in line with reports indicating that the MyHC isoform expression is the main determinant of contractility and power output of the heart (Herron and McDonald, 2002; Palmiter et al., 1999). Independent of Ca^{2+} handling, the expression of the MyHC isoforms was shown to determine sarcomere shortening amplitude and velocity (Herron et al., 2007, 2010). Interestingly, the shift from predominant β-MyHC to mixed α-/β-MyHC expression seems to be mainly driven by substantially increased expression of *MYH6* and only slightly by downregulation of *MYH7*. This rather preserved *MYH7* mRNA expression might facilitate the retransition to mainly β-MyHC expressing cells within 1–2 wk after replating.

A shift in MyHC isoform protein expression can account for changes in myofibrillar force-related kinetic parameters but not necessarily for the decrease in force generation after replating. In line, the duty ratio ($f_{app}/f_{app} + g_{app}$), considered to modulate kinetically the steady state force level, was relatively constant for both replated (35 + 2 d: 0.67 ± 0.15; 35 + 9 d: 0.63 ± 0.14) and non-replated (35 d: 0.64 ± 0.08) CMs. Therefore, other factors, such as extensive sarcomeric remodeling, could potentially contribute to the force decrease. Furthermore, the functional characteristics of CMs are also influenced by the expression of distinct isoforms of other sarcomeric proteins (Iorga et al., 2018). Interestingly, replating-related changes in the mRNA expression of *MYL* and *TNN* isoforms were not as profound as the changes in *MYH6* isoform expression. Nevertheless, our data do not exclude either changes in protein expression of MLCs (especially ventricular, see Fig. 5 F) or of Z-disk components that might affect isometric force after replating.

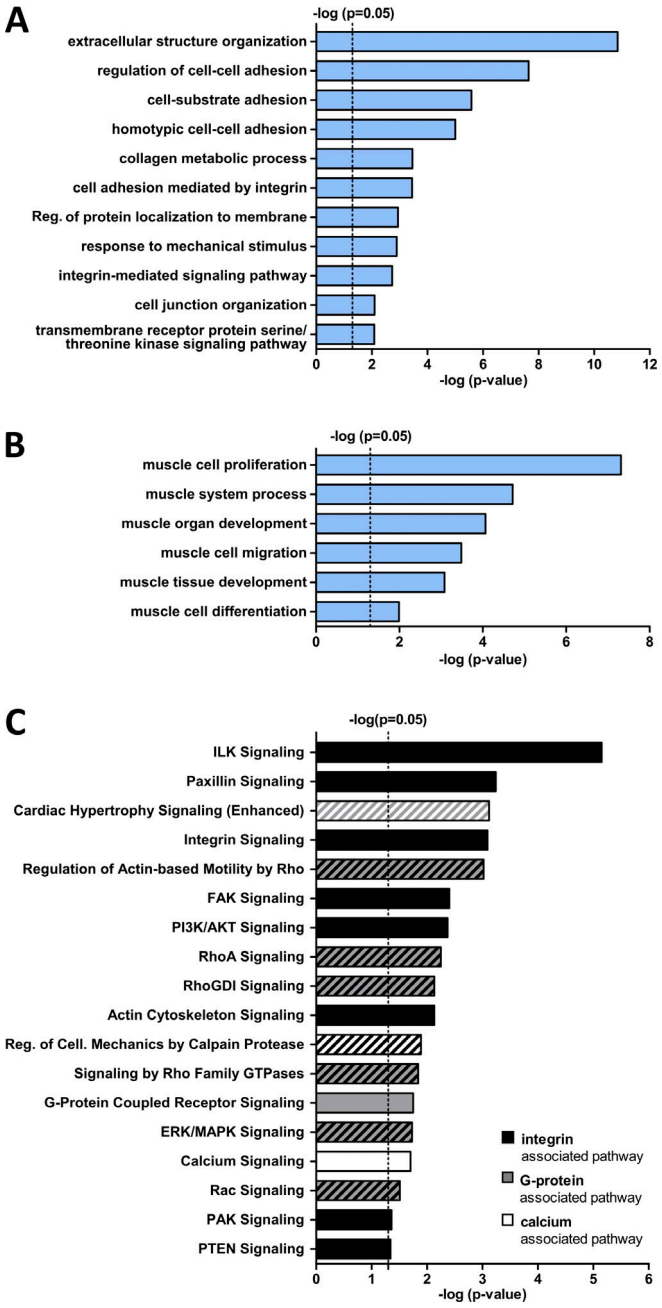

Figure 6. **Gene enrichment analysis based on RNA-seq data of replated (35 + 2 d) vs. non-replated control (37 d) hESC-CMs.** hESC-CMs grown for 35 d on laminin-coated glass coverslips were detached, replated on laminin-coated glass coverslips, and grown for an additional 2 d. Gene expression was compared with 37-d-old controls (fold change cutoff 1.5; $n = 3$). **(A and B)** Enriched biological process categories related to (A) ECM and cell adhesion, and (B) muscle development and function as demonstrated by GO analysis of upregulated genes using the functional enrichment analysis web tool WebGestalt. Sorted by –log P value ranking (Fisher's exact test) with $P < 0.05$ set as the threshold. **(C)** IPA (Qiagen) revealed canonical pathways involved in mechanosensation/-transduction. Integrin-, G-protein- and calcium-associated pathways are indicated with a threshold of $P < 0.05$. Significance values (P value of overlap) for canonical pathways are calculated by the right-tailed Fisher's exact test; $n = 3$ culture dishes from three differentiations. Combinations of black-, white-, or gray-striped bars refer to the involvement of signaling in two of the pathway categories as indicated by the legend.

Changes in ECM stiffness, i.e., a reduced mechanical load or stress after detachment of the long-term plated hESC-CMs, most likely, induced the observed changes in protein and gene expression, and thereby function. This conclusion is supported by the finding of changes in mechanosensation/-transduction-related gene expression, including integrin-related signaling as indicated by GO and IPA analysis based on RNA-Seq data. GO analyses demonstrated several enriched categories related to ECM organization and cell interaction, presumably reflecting effects that result from changes in matrix stiffness. It has been shown that substrate stiffness affects the mechanosensing and signaling pathways of CMs in heart development and growth (Gaetani et al., 2020; Munch and Abdelilah-Seyfried, 2021). The costameres, a complex network of proteins that connects the ECM to the sarcomeres, form the structural basis of mechanotransduction (Harvey and Leinwand, 2011). Cardiomyocyte function has been shown to be affected by several mechanosensation/-transduction pathways that are related to integrins, G-protein-coupled receptors, and calcium channels (Dostal et al., 2014). Changes in ECM stiffness can be sensed by integrins and transmitted via integrin-dependent pathways including FAK (Pentassuglia and Sawyer, 2013). FAK overexpression in mice has been demonstrated to induce concentric hypertrophy with increased *MYH7* mRNA expression (Clemente et al., 2012). Integrin-dependent mechanosensation can also occur at the intercalated disc (Pruna and Ehler, 2020). Furthermore, changes in the mechanical load can also be sensed by structures in the sarcomere, with the protein phosphatase calcineurin as an important downstream mediator (Linke and Knöll, 2010; Lyon et al., 2015) that can affect *MYH7* expression at least under hypertrophic conditions (Molkentin et al., 1998). Data from IPA canonical pathway analysis and pharmacological interference experiments with replated hESC-CMs (not shown) suggest that integrin, but not calcium signaling, is primarily involved in replating-related changes in gene expression. In accordance with GO and IPA analysis, we could demonstrate that integrin downstream mediator FAK is involved in the regulation of β-MyHC expression, indicating the relevance of mechanosensation/-transduction for matrix-induced changes. Interestingly, a higher concentration (10 μM) of the FAK inhibitor 14 was shown to decrease β-MyHC expression in hiPSC-CMs grown on Matrigel-coated PDMS (Herron et al., 2016), a softer matrix compared with laminin-coated glass coverslips. In hESC-CMs, the effect of FAK on MyHC expression was not mediated by ERK1/2 MAPK. Thus, the precise mechanism of integrin signaling mediating the effects of replating in general and especially on *MYH*/MyHC isoform expression remains to be determined.

Applying increased afterload, hiPSC-CMs grown in engineered heart tissue (EHT) were subjected to increased mechanical load. It has been shown that hiPSC-CMs responded at the molecular level (Leonard et al., 2018). Increased afterload led to an increased ratio of *MYH7*/*MYH6* mRNA and β-/α-MyHC protein as well as increased expression of other cardiac-specific sarcomeric genes, thus promoting maturation. Under the highest afterload conditions, the expression of the mechanosensitive muscle-specific chaperone melusin (*ITGB1BP2*) was also increased. These findings demonstrate that also in 3-D culture

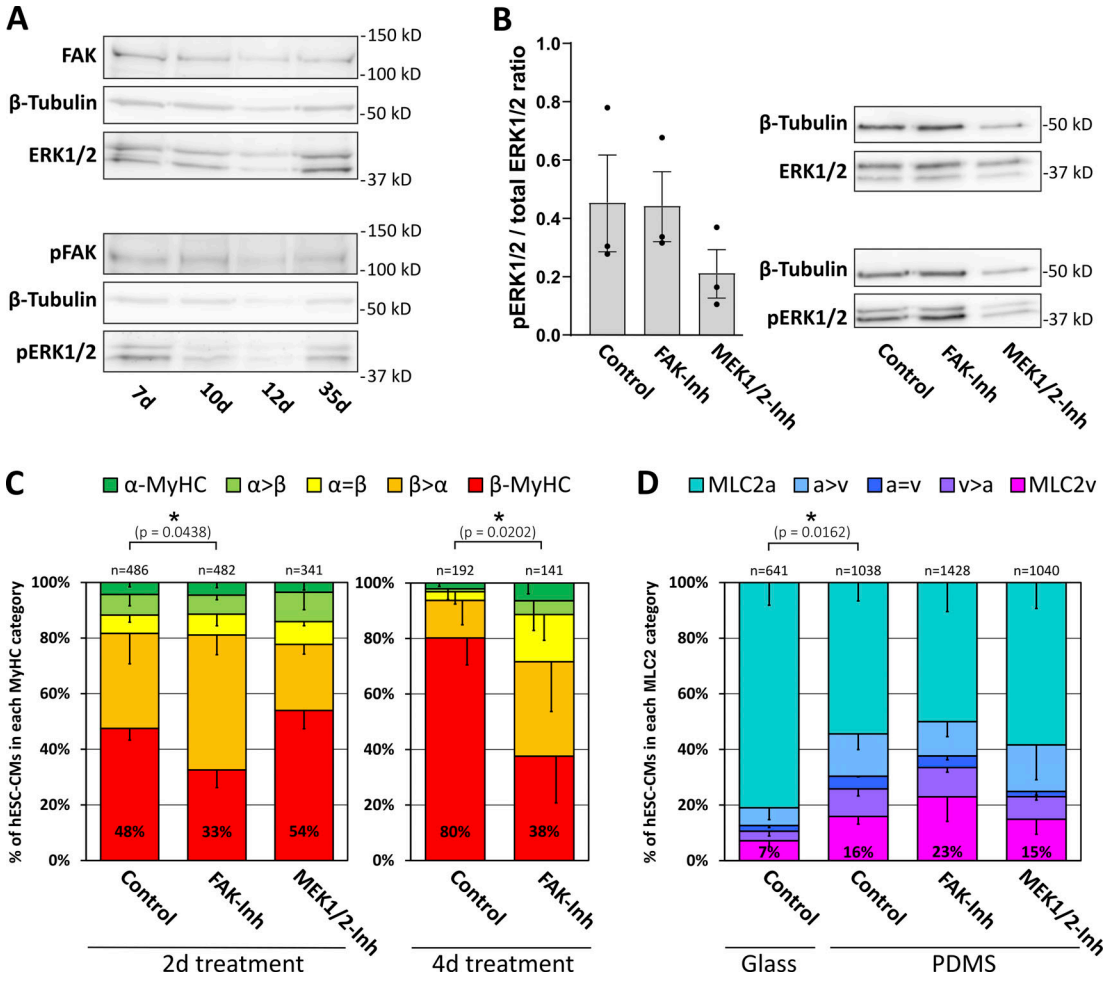

Figure 7. **β-MyHC expression is reduced by inhibition of FAK. (A)** Western blot analysis of FAK and ERK1/2-MAPK expression and phosphorylation in hESC-CMs grown for indicated days on laminin-coated glass coverslips. Representative blot, with β-tubulin serving as a loading control. **(B)** Western blot analysis of ERK1/2-MAPK phosphorylation in 35 d hESC-CMs grown on Matrigel-coated PDMS treated with or without 5 µM FAK-inhibitor 14 (FAK-Inh) or 10 µM MEK1/2 inhibitor U0126 (MEK1/2-Inh) for 2 d. The ratio of phospho/total ERK1/2-MAPK expression was determined densitometrically. Mean ± SEM; *n* = 3 individual coverslips from one differentiation. Representative blot, with β-tubulin serving as a loading control. **(C)** Myosin isoform expression was analyzed by single-cell IF using specific antibodies against α-MyHC and β-MyHC in hESC-CMs grown on laminin-coated glass coverslips treated with or without 5 µM FAK-inhibitor 14 (FAK-Inh) or 10 µM MEK1/2 inhibitor U0126 (MEK1/2-Inh) from day 7 on for 2 or 4 d. The fractions of cells in the different indicated categories (see Materials and methods) are shown as a percentage of the total number of cells analyzed (*n*, set to 100%, from three coverslips derived from one differentiation; P values: exclusively β-MyHC expressing cells. **(D)** hESC-CMs were grown for 35 d on laminin-coated glass coverslips or on Matrigel-coated PDMS and treated with or without 5 µM FAK-inhibitor 14 (FAK-Inh) or 10 µM MEK1/2 inhibitor U0126 (MEK1/2-Inh) for 2 d as indicated. MLC2 isoform expression was analyzed by single-cell IF using specific antibodies against MLC2v and MLC2a. The fractions of cells in the different categories (see Materials and methods) are shown as a percentage of the total number of cells analyzed (*n*, set to 100%, from three coverslips derived from one differentiation; P values: exclusively MLC2v expressing cells). Source data are available for this figure: SourceData F7.

mechanical load can induce changes in sarcomeric gene expression, presumably mediated by mechanosensation/-transduction. Notably, a different study with EHTs showed a strong correlation between the MyHC isoform ratio with shortening velocity, demonstrating that increased amounts of shortening or contractile work induced an increase in the relative abundance of α-MyHC in hiPSC-CMs (Ng et al., 2021).

To conclude, the presented data demonstrate that stiffness changes of the matrix in the context of detaching and replating hPSC-CMs for functional measurements lead to changes in mechanosensation/-transduction. Altered mechanosensation/-transduction involving integrin-related signaling is assumed to be causal for the observed rapid shift from predominant β-MyHC-expression to upregulation of α-MyHC expression as well as accompanying alterations in contractile function and calcium transients. It takes at least 1 wk of cultivation after replating to essentially reverse the induced changes in MyHC isoform expression and contractile function. These changes should be taken into account when hPSC-CMs are detached and replated particularly for downstream in vitro assays.

Data availability

RNA-sequencing datasets associated with this article can be downloaded from GEO under accession no. GSE176154. Datasets generated or analyzed during this study, if not already included in this article, as well as raw data, are available upon reasonable

request by contacting F. Osten (osten.felix@mh-hannover.de) or T. Kraft (kraft.theresia@mh-hannover.de).

Acknowledgments

Henk L. Granzier served as editor.

We thank Prof. Dr. Denise Hilfiker-Kleiner (Department of Cardiology and Angiology, Hannover Medical School, Hannover, Germany; present address: Department of Cardiovascular Complications of Oncologic Therapies, Philipps University Marburg, Marburg, Germany) for providing human myocardial samples, Dr. Oliver Dittrich-Breiholz and Dr. Ante Radocaj for helpful discussions, and Heike Schneider for excellent technical assistance. Sequencing data used or referred to in this publication were generated by the Research Core Unit Genomics (RCUG) at Hannover Medical School.

The presented work was supported by grants from Deutsche Forschungsgemeinschaft (DFG: BR849/31-1, KR1187/21-1). The work was additionally supported by grants to R Zweigerdt: DFG (Cluster of Excellence REBIRTH EXC 62/2, ZW64/4-2, KFO311/ZW64/7-1), the Federal Ministry of Education and Research (BMBF, 01EK1601A, 13XP5092B, 031L0249, and 01EK2108A), Lower Saxony "Förderung aus Mitteln des Niedersächsischen Vorab"(ZN3340), and the European Union (EU Horizon project HEAL, 101056712; views and opinions expressed are however those of the author(s) only and do not necessarily reflect those of the European Union or the European Health and Digital Executive Agency (HADEA). Neither the European Union nor the granting authority can be held responsible for them). Parts of that work were additionally funded by DFG TRR267 (to T. Thum) and CRC1470 (to T. Thum).

T. Thum filed and licensed patents in the field of noncoding RNAs and is the founder and shareholder of Cardior Pharmaceuticals GmbH.

Author contributions: F. Osten: conceptualization, investigation, formal analysis, visualization, writing - review and editing; N. Weber: conceptualization, investigation, formal analysis, visualization, writing - review and editing; M. Wendland: investigation, formal analysis; T. Holler: investigation, visualization; B. Piep: investigation; S. Kröhn: investigation; J. Teske: resources; A. Bodenschatz: investigation; S. Biswanath Devadas: resources; K. Menge: resources; S. Chatterjee: resources; K. Schwanke: resources; M. Kosanke: data curation, formal analysis; J. Montag: conceptualization, writing - review and editing; T. Thum: resources, funding acquisition; R. Zweigerdt: resources, funding acquisition; T. Kraft: conceptualization, funding acquisition, supervision, writing - review and editing; B. Iorga: conceptualization, investigation, formal analysis, writing - review and editing; J. Meissner: conceptualization, investigation, project administration, writing - original draft, review and editing.

Disclosures: T. Thum reported other from Cardior Pharmaceuticals outside the submitted work. No other disclosures were reported.

Submitted: 1 March 2023
Revised: 16 June 2023
Accepted: 19 July 2023

References

Brenner, B. 1988. Effect of Ca2+ on cross-bridge turnover kinetics in skinned single rabbit psoas fibers: Implications for regulation of muscle contraction. *Proc. Natl. Acad. Sci. USA*. 85:3265–3269. https://doi.org/10.1073/pnas.85.9.3265

Castillo, E.A., K.V. Lane, and B.L. Pruitt. 2020. Micromechanobiology: Focusing on the cardiac cell-substrate interface. *Annu. Rev. Biomed. Eng.* 22:257–284. https://doi.org/10.1146/annurev-bioeng-092019-034950

Chatterjee, S., T. Hofer, A. Costa, D. Lu, S. Batkai, S.K. Gupta, E. Bolesani, R. Zweigerdt, D. Megias, K. Streckfuss-Bömeke, et al. 2021. Telomerase therapy attenuates cardiotoxic effects of doxorubicin. *Mol. Ther.* 29:1395–1410. https://doi.org/10.1016/j.ymthe.2020.12.035

Clemente, C.F., J. Xavier-Neto, A.P. Dalla Costa, S.R. Consonni, J.E. Antunes, S.A. Rocco, M.B. Pereira, C.C. Judice, B. Strauss, P.P. Joazeiro, et al. 2012. Focal adhesion kinase governs cardiac concentric hypertrophic growth by activating the AKT and mTOR pathways. *J. Mol. Cell. Cardiol.* 52:493–501. https://doi.org/10.1016/j.yjmcc.2011.10.015

Denning, C., V. Borgdorff, J. Crutchley, K.S. Firth, V. George, S. Kalra, A. Kondrashov, M.D. Hoang, D. Mosqueira, A. Patel, et al. 2016. Cardiomyocytes from human pluripotent stem cells: From laboratory curiosity to industrial biomedical platform. *Biochim. Biophys. Acta*. 1863:1728–1748. https://doi.org/10.1016/j.bbamcr.2015.10.014

Dostal, D.E., H. Feng, D. Nizamutdinov, H.B. Golden, S.H. Afroze, J.D. Dostal, J.C. Jacob, D.M. Foster, C. Tong, S. Glaser, and F. Gerilechaogetu. 2014. Mechanosensing and regulation of cardiac function. *J. Clin. Exp. Cardiolog.* 5:314, https://doi.org/10.4172/2155-9880.1000314

Gaetani, R., E.A. Zizzi, M.A. Deriu, U. Morbiducci, M. Pesce, and E. Messina. 2020. When stiffness matters: Mechanosensing in heart development and disease. *Front. Cell Dev. Biol.* 8:334. https://doi.org/10.3389/fcell.2020.00334

Haase, A., G. Göhring, and U. Martin. 2017. Generation of non-transgenic iPS cells from human cord blood CD34$^+$ cells under animal component-free conditions. *Stem Cell Res.* 21:71–73. https://doi.org/10.1016/j.scr.2017.03.022

Harvey, P.A., and L.A. Leinwand. 2011. The cell biology of disease: Cellular mechanisms of cardiomyopathy. *J. Cell Biol.* 194:355–365. https://doi.org/10.1083/jcb.201101100

Herron, T.J., E. Devaney, L. Mundada, E. Arden, S. Day, G. Guerrero-Serna, I. Turner, M. Westfall, and J.M. Metzger. 2010. Ca2+-independent positive molecular inotropy for failing rabbit and human cardiac muscle by alpha-myosin motor gene transfer. *FASEB J.* 24:415–424. https://doi.org/10.1096/fj.09-140566

Herron, T.J., and K.S. McDonald. 2002. Small amounts of alpha-myosin heavy chain isoform expression significantly increase power output of rat cardiac myocyte fragments. *Circ. Res.* 90:1150–1152. https://doi.org/10.1161/01.RES.0000022879.57270.11

Herron, T.J., A.M. Rocha, K.F. Campbell, D. Ponce-Balbuena, B.C. Willis, G. Guerrero-Serna, Q. Liu, M. Klos, H. Musa, M. Zarzoso, et al. 2016. Extracellular matrix-mediated maturation of human pluripotent stem cell-derived cardiac monolayer structure and electrophysiological function. *Circ. Arrhythm. Electrophysiol.* 9:e003638. https://doi.org/10.1161/CIRCEP.113.003638

Herron, T.J., R. Vandenboom, E. Fomicheva, L. Mundada, T. Edwards, and J.M. Metzger. 2007. Calcium-independent negative inotropy by beta-myosin heavy chain gene transfer in cardiac myocytes. *Circ. Res.* 100:1182–1190. https://doi.org/10.1161/01.RES.0000264102.00706.4e

Iorga, B., K. Schwanke, N. Weber, M. Wendland, S. Greten, B. Piep, C.G. Dos Remedios, U. Martin, R. Zweigerdt, T. Kraft, and B. Brenner. 2018. Differences in contractile function of myofibrils within human embryonic stem cell-derived cardiomyocytes vs. Adult ventricular myofibrils are related to distinct sarcomeric protein isoforms. *Front. Physiol.* 8:1111. https://doi.org/10.3389/fphys.2017.01111

Israeli-Rosenberg, S., A.M. Manso, H. Okada, and R.S. Ross. 2014. Integrins and integrin-associated proteins in the cardiac myocyte. *Circ. Res.* 114:572–586. https://doi.org/10.1161/CIRCRESAHA.114.301275

Jiang, Y., P. Park, S.M. Hong, and K. Ban. 2018. Maturation of cardiomyocytes derived from human pluripotent stem cells: Current strategies and limitations. *Mol. Cells*. 41:613–621. https://doi.org/10.14348/molcells.2018.0143

Koc, A., S. Sahoglu Goktas, T. Akgul Caglar, and E. Cagavi. 2021. Defining optimal enzyme and matrix combination for replating of human induced pluripotent stem cell-derived cardiomyocytes at different levels of maturity. *Exp. Cell Res.* 403:112599. https://doi.org/10.1016/j.yexcr.2021.112599

Kraft, T., E.R. Witjas-Paalberends, N.M. Boontje, S. Tripathi, A. Brandis, J. Montag, J.L. Hodgkinson, A. Francino, F. Navarro-Lopez, B. Brenner,

et al. 2013. Familial hypertrophic cardiomyopathy: Functional effects of myosin mutation R723G in cardiomyocytes. *J. Mol. Cell. Cardiol.* 57: 13–22. https://doi.org/10.1016/j.yjmcc.2013.01.001

Kreutzer, F.P., A. Meinecke, S. Mitzka, H.J. Hunkler, L. Hobuß, N. Abbas, R. Geffers, J. Weusthoff, K. Xiao, D.D. Jonigk, et al. 2022. Development and characterization of anti-fibrotic natural compound similars with improved effectivity. *Basic Res. Cardiol.* 117:9. https://doi.org/10.1007/s00395-022-00919-6

Leonard, A., A. Bertero, J.D. Powers, K.M. Beussman, S. Bhandari, M. Regnier, C.E. Murry, and N.J. Sniadecki. 2018. Afterload promotes maturation of human induced pluripotent stem cell derived cardiomyocytes in engineered heart tissues. *J. Mol. Cell. Cardiol.* 118:147–158. https://doi.org/10.1016/j.yjmcc.2018.03.016

Liao, Y., J. Wang, E.J. Jaehnig, Z. Shi, and B. Zhang. 2019. WebGestalt 2019: Gene set analysis toolkit with revamped UIs and APIs. *Nucleic Acids Res.* 47:W199–W205. https://doi.org/10.1093/nar/gkz401

Linke, W.A., and R.H. Knöll. 2010. Cardiac mechanosensation and clinical implications. *Eur. J. Cardiovasc. Med.* 1:33–37.

Locher, M.R., M.V. Razumova, J.E. Stelzer, H.S. Norman, J.R. Patel, and R.L. Moss. 2009. Determination of rate constants for turnover of myosin isoforms in rat myocardium: Implications for in vivo contractile kinetics. *Am. J. Physiol. Heart Circ. Physiol.* 297:H247–H256. https://doi.org/10.1152/ajpheart.00922.2008

Lyon, R.C., F. Zanella, J.H. Omens, and F. Sheikh. 2015. Mechanotransduction in cardiac hypertrophy and failure. *Circ. Res.* 116:1462–1476. https://doi.org/10.1161/CIRCRESAHA.116.304937

Maltsev, V.A., A.M. Wobus, J. Rohwedel, M. Bader, and J. Hescheler. 1994. Cardiomyocytes differentiated in vitro from embryonic stem cells developmentally express cardiac-specific genes and ionic currents. *Circ. Res.* 75:233–244. https://doi.org/10.1161/01.RES.75.2.233

Molkentin, J.D., J.R. Lu, C.L. Antos, B. Markham, J. Richardson, J. Robbins, S.R. Grant, and E.N. Olson. 1998. A calcineurin-dependent transcriptional pathway for cardiac hypertrophy. *Cell.* 93:215–228. https://doi.org/10.1016/S0092-8674(00)81573-1

Münch, J., and S. Abdelilah-Seyfried. 2021. Sensing and responding of cardiomyocytes to changes of tissue stiffness in the diseased heart. *Front. Cell Dev. Biol.* 9:642840. https://doi.org/10.3389/fcell.2021.642840

Ng, R., L.R. Sewanan, P. Stankey, X. Li, Y. Qyang, and S. Campbell. 2021. Shortening velocity causes myosin isoform shift in human engineered heart tissues. *Circ. Res.* 128:281–283. https://doi.org/10.1161/CIRCRESAHA.120.316950

Palmiter, K.A., M.J. Tyska, D.E. Dupuis, N.R. Alpert, and D.M. Warshaw. 1999. Kinetic differences at the single molecule level account for the functional diversity of rabbit cardiac myosin isoforms. *J. Physiol.* 519: 669–678. https://doi.org/10.1111/j.1469-7793.1999.0669n.x

Pentassuglia, L., and D.B. Sawyer. 2013. ErbB/integrin signaling interactions in regulation of myocardial cell-cell and cell-matrix interactions. *Biochim. Biophys. Acta.* 1833:909–916. https://doi.org/10.1016/j.bbamcr.2012.12.007

Pruna, M., and E. Ehler. 2020. The intercalated disc: A mechanosensing signalling node in cardiomyopathy. *Biophys. Rev.* 12:931–946. https://doi.org/10.1007/s12551-020-00737-x

Reiser, P.J., M.A. Portman, X.H. Ning, and C. Schomisch Moravec. 2001. Human cardiac myosin heavy chain isoforms in fetal and failing adult atria and ventricles. *Am. J. Physiol. Heart Circ. Physiol.* 280:H1814–H1820. https://doi.org/10.1152/ajpheart.2001.280.4.H1814

Ren, X.D., R. Wang, Q. Li, L.A. Kahek, K. Kaibuchi, and R.A. Clark. 2004. Disruption of Rho signal transduction upon cell detachment. *J. Cell Sci.* 117:3511–3518. https://doi.org/10.1242/jcs.01205

Rundell, V.L., V. Manaves, A.F. Martin, and P.P. de Tombe. 2005. Impact of beta-myosin heavy chain isoform expression on cross-bridge cycling kinetics. *Am. J. Physiol. Heart Circ. Physiol.* 288:H896–H903. https://doi.org/10.1152/ajpheart.00407.2004

Sadoshima, J., and S. Izumo. 1997. The cellular and molecular response of cardiac myocytes to mechanical stress. *Annu. Rev. Physiol.* 59:551–571. https://doi.org/10.1146/annurev.physiol.59.1.551

Santoro, R., G.L. Perrucci, A. Gowran, and G. Pompilio. 2019. Unchain my heart: Integrins at the basis of iPSC cardiomyocyte differentiation. *Stem Cells Int.* 2019:8203950. https://doi.org/10.1155/2019/8203950

Saucerman, J.J., P.M. Tan, K.S. Buchholz, A.D. McCulloch, and J.H. Omens. 2019. Mechanical regulation of gene expression in cardiac myocytes and fibroblasts. *Nat. Rev. Cardiol.* 16:361–378. https://doi.org/10.1038/s41569-019-0155-8

Schwanke, K., S. Merkert, H. Kempf, S. Hartung, M. Jara-Avaca, C. Templin, G. Göhring, A. Haverich, U. Martin, and R. Zweigerdt. 2014. Fast and efficient multitransgenic modification of human pluripotent stem cells. *Hum. Gene Ther. Methods.* 25:136–153. https://doi.org/10.1089/hgtb.2012.248

Schwartz, K., Y. Lecarpentier, J.L. Martin, A.M. Lompré, J.J. Mercadier, and B. Swynghedauw. 1981. Myosin isoenzymic distribution correlates with speed of myocardial contraction. *J. Mol. Cell. Cardiol.* 13:1071–1075. https://doi.org/10.1016/0022-2828(81)90297-2

Weber, N., K. Kowalski, T. Holler, A. Radocaj, M. Fischer, S. Thiemann, J. de la Roche, K. Schwanke, B. Piep, N. Peschel, et al. 2020. Advanced single cell mapping reveals that in hESC-cardiomyocytes contraction kinetics and action potential are independent of myosin isoform. *Stem Cell Rep.* 14:788–802. https://doi.org/10.1016/j.stemcr.2020.03.015

Weber, N., K. Schwanke, S. Greten, M. Wendland, B. Iorga, M. Fischer, C. Geers-Knörr, J. Hegermann, C. Wrede, J. Fiedler, et al. 2016. Stiff matrix induces switch to pure β-cardiac myosin heavy chain expression in human ESC-derived cardiomyocytes. *Basic Res. Cardiol.* 111:68. https://doi.org/10.1007/s00395-016-0587-9

World Medical Association. 2013. World Medical Association Declaration of Helsinki: ethical principles for medical research involving human subjects. *JAMA.* 310:2191–2194. https://doi.org/10.1001/jama.2013.281053

Xu, X.Q., R. Zweigerdt, S.Y. Soo, Z.X. Ngoh, S.C. Tham, S.T. Wang, R. Graichen, B. Davidson, A. Colman, and W. Sun. 2008. Highly enriched cardiomyocytes from human embryonic stem cells. *Cytotherapy.* 10: 376–389. https://doi.org/10.1080/14653240802105307

Yang, X., L. Pabon, and C.E. Murry. 2014. Engineering adolescence: Maturation of human pluripotent stem cell-derived cardiomyocytes. *Circ. Res.* 114:511–523. https://doi.org/10.1161/CIRCRESAHA.114.300558